Atmospheric Environment 152 (2017) 330–344

Contents lists available at ScienceDirect

Atmospheric Environment

journal homepage: www.elsevier.com/locate/atmosenv

Submicron particle dynamics for different surfaces under quiescent and turbulent conditions

Karn Vohra [a], Kunal Ghosh [a], S.N. Tripathi [a, b, *], I. Thangamani [c], P. Goyal [c], Anu Dutta [c], V. Verma [c]

[a] Department of Civil Engineering, Indian Institute of Technology Kanpur, Kanpur 208016, Uttar Pradesh, India
[b] Centre for Environmental Science and Engineering, IIT Kanpur, 208016, India
[c] Reactor Safety Division, Bhabha Atomic Research Centre, Trombay, Maharashtra, India

HIGHLIGHTS

- Modeling both coagulation and deposition to predict aerosol behavior accurately.
- Both coagulation and deposition are significant for submicron particles.
- Surface roughness and turbulence have a cumulative effect in increasing deposition.
- Increasing turbulence helps reduce aerosol peak concentration faster.

ARTICLE INFO

Article history:
Received 25 March 2016
Received in revised form
3 December 2016
Accepted 5 December 2016
Available online 12 December 2016

Keywords:
Coagulation
Deposition
Submicron
Turbulence

ABSTRACT

Experiments were conducted using CsI aerosols in a small scale test chamber to simulate behaviour of aerosols in the containment of a nuclear reactor. The primary focus of the study was on submicron particles (14.3 nm–697.8 nm) due to their hazardous effect on human health. Different wall surfaces, viz., plexiglass, concrete and sandpaper were chosen to study the effect of surface roughness on dry deposition velocity under both quiescent and turbulent conditions. An analytical approach to calculate dry deposition velocity of submicron particles for rough surfaces has been proposed with an improvement in the existing parameterization for shift in the velocity boundary layer. The predicted deposition velocity with the improved parameterization was found to have better agreement with published measured data of Lai and Nazaroff (2005) compared to the existing parameterizations (Wood, 1981; Zhao and Wu, 2006b). There was a significant reduction in root mean square error (RMSE) between predicted, using the improved parameterization and measured deposition velocity (upto 100%) compared to earlier ones. The new analytical deposition approach was coupled with volume conserving semi-implicit coagulation model. This aerosol dynamic model was evaluated against explicit particle size distribution for the first time for rough surfaces. Normalized RMSE between simulated and measured particle size distribution varied in the range of 2%–20% at different instances. The model seems to closely predict submicron particle behaviour in indoor environment.

1. Introduction

In a nuclear reactor, under postulated accident conditions, the cooling to the reactor fuel can be lost and the fuel gets overheated. This overheating can lead to fuel damage causing release of radioactive fission products in the form of aerosols (Sapra et al., 2008). These aerosols get transported through the broken coolant system and reach the containment which is the final barrier in their release to the public domain. The study of the behaviour of aerosols in the containment is a subject of research worldwide (Fischer and Kanzleiter, 1999). These studies are important to characterize the source term into the environment so that the effect of radioactivity in the public domain can be quantified and possibly mitigated by confinement within the containment. The aerosol particles released during such scenarios are reported to have a diameter in the size range of 0.1 μm–20 μm, covering both the continuum and

* Corresponding author.
E-mail address: snt@iitk.ac.in (S.N. Tripathi).

http://dx.doi.org/10.1016/j.atmosenv.2016.12.013
1352-2310/

Nomenclature

A	Surface area (m^2)
β	Coagulation kernel ($m^3\ s^{-1}$)
b	Effective roughness height (μm)
C	Particle number concentration (cm^{-3})
D	Brownian diffusivity of particle ($cm^2\ s^{-1}$)
d	Particle diameter (nm)
e	Shift in velocity boundary layer (μm)
e^+	Dimensionless parameter for shift in velocity boundary layer
ε	Turbulent (eddy) diffusivity of particle ($cm^2\ s^{-1}$)
$f_{i,j,k}$	Volume fraction of colliding particles of bin i & j partitioned into bin k
J	Particle flux given by Fick's law ($cm^{-2}\ s^{-1}$)
k^+	Dimensionless surface roughness height
k_s	Mean surface roughness height (μm)
Q	Sampling rate of instruments ($m^3\ s^{-1}$)
r^+	Dimensionless radius of particle
Sc	Schmidt number
t	Time (s)
u^*	Friction velocity ($cm\ s^{-1}$)
V	Chamber volume (m^3)
v	Volume of a particular size bin (m^3)
v	Velocity of particle ($cm\ s^{-1}$)
λ	Ventilation rate (h^{-1})
τ	Particle relaxation time (s)
Δt	Time step (s)
ν	Fluid kinematic viscosity ($m^2\ s^{-1}$)
y	Distance from the wall or surface (μm)

Subscripts

ceil	Ceiling (top surface of the chamber)
floor	Floor (base of the chamber)
wall	Vertical walls of the chamber
d	Deposition
p	Particle
s	Settling
t	Turbulent

slip flow regimes (Brockmann and Tarbell, 1984). From a health perspective, the submicron particles are of great concern due to their high number density, and ability to penetrate deep into the lungs and induce oxidative stress with cellular damage (Song et al., 2011). Natural attenuation of radioactive material occurs due to deposition of aerosols on the internal surface of a reactor (Slama et al., 2014). The aerosol inventory in the containment atmosphere depends on the aerosol released into the containment and aerosol removal processes like deposition, gravitational sedimentation, and leaks.

Deposition of particles onto the indoor surfaces of the reactor can effectively reduce the exposure to harmful aerosols unless resuspended. The essential mechanisms for deposition in the nuclear containment have been listed as Brownian and turbulent diffusion, turbophoresis, gravitational sedimentation, thermophoresis, convective transfer due to condensation of the vapours on the inner surface of the reactor, and centrifugal force in case of flow around a curved surface (Simons and Simpson, 1988; Alipchenkov et al., 2009).

Crump and Seinfeld (1981) derived a general formula for rate of aerosol deposition due to Brownian and turbulent diffusion as well as gravitational sedimentation in a turbulently mixed vessel. However, this model is valid when the inertial effects are insignificant. Indoor particle deposition onto smooth surfaces was modelled in Lai and Nazaroff (2000) and Mayya et al. (2004) taking into account deposition only due to Brownian diffusion, turbulent diffusion, and gravitational settling. A modified version of this model (popularly known as the three-layer model), taking turbophoresis also into consideration, has been proposed (Zhao and Wu, 2006a). It is an improved model, which correctly models the three different zones classified according to the particle relaxation times (turbulent diffusion regime, turbulent diffusion-eddy impaction regime, and particle inertia moderated regime).

Deposition onto rough surfaces has been studied both experimentally and theoretically, and similar trends of increase in deposition velocity with increase in particle sizes, turbulence and size of roughness were observed (Shimada et al., 1988; Shimada et al., 1989; Zhao and Wu, 2007; Hussein et al., 2009a,b). However, the numerical model proposed by Shimada et al. (1988) focused only on diffusion ignoring the gravitational sedimentation. Experimental studies were done in a 8 m^3 test chamber facility and they also showed similar results (Lai et al., 2002). Particle deposition on rough surfaces was found to be less than that on the smooth surfaces for small particles and low airflow condition. For large size particles and high airflow conditions, particle deposition on rough surfaces increased upto three times to that on smooth surfaces. Experimental studies for particle deposition in ventilation ducts have been carried out and the results modelled by applying a roughness of 180 μm as opposed to the hydraulic roughness of about 1600 μm measured by the axial pressure drop in the ventilation ducts (Sippola and Nazaroff, 2004). Wood (1981) assumed that for a rough surface, the virtual origin of the velocity profile is shifted by a distance $e(=0.55k_s)$ away from the wall, where k_s is the roughness height. This was incorporated in the boundary condition in the three-layer model of Lai and Nazaroff (2000) in order to study coarse particle deposition onto rough surfaces (Lai, 2005). Experiments were carried out using four sandpapers with different roughness scales (Lai and Nazaroff, 2005), but the model predicted satisfactory results only for the finer sandpapers. Zhao and Wu (2006b) have modelled particle deposition onto rough surfaces in ventilation ducts as an improvement of the three-layer model proposed in Zhao & Wu, (2006a) by incorporating surface roughness in the boundary condition. A new equation stated in Eq. (1) was fitted on the experimental data of Grass (1971) and Wan (1981) in order to calculate the shifted distance in the boundary layer (Zhao and Wu, 2006b). Both e^+ and k^+ are dimensionless parameters, which are described later in detail (Section 2.2.2).

$$\frac{e^+}{k^+} = \begin{cases} 0 & k^+ < 3 \quad \text{Hydraulically smooth} \\ 0.3219\ln(k^+) - 0.3456 & 3 < k^+ < 30 \quad \text{Transition} \\ 0.0835\ln(k^+) + 0.4652 & 30 < k^+ < 70 \quad \text{Transition} \\ 0.82 & k^+ > 70 \quad \text{Completely rough} \end{cases} \tag{1}$$

The results predicted by the improved model agreed better with the measured data of Sippola and Nazaroff (2004) than the traditional model suggested by Wood (1981), but were not satisfactory. It was suggested that this may be due to the fact that Eq. (1) was obtained under the condition that the roughness was made up by

uniformly distributed balls and that the roughness was far more complicated in the experiments of Sippola and Nazaroff (2004). Therefore, the accurate value of the shift distance might be different due to different kind of roughness. However, most of these studies overpredicted the dry deposition velocity for a rough surface to a great extent. Moreover, none of the studies have concentrated on the evolution of aerosol particles with time in case of rough surfaces.

In another study, semi-empirical expressions were obtained for evaluating dry deposition velocities on vertical and horizontal surfaces, which significantly reducing the dry deposition velocity overpredictions (Piskunov, 2009). Another approach used a hybrid parameter that included both the surface roughness height and the peak-to-peak distance between roughness elements (Huessin et al., 2012). This new approach predicts dry deposition velocities over most surfaces and covers a wide size range of aerosol particles. However, this approach needs to be further developed and information about peak-to-peak distance between roughness elements should be available for each surface type.

Experimental chamber studies have also been conducted to study collectively both coagulation and deposition of polydisperse (NaCl) nanoparticles with size ranging from 30 nm to 120 nm (Kim et al., 2006). It was found that in case of high number concentrations, coagulation played a more significant role as compared to deposition (Anand et al., 2012). In addition to studying both coagulation and deposition in a chamber, the effect of turbulence was also investigated for combustion aerosols by studying the number concentration decay and the variation of particle size distributions (size range of 0.016 μm–20 μm) with time for both quiescent and turbulent conditions (Schnell et al., 2006). It was observed that coagulation dominated concentration decay under still conditions. In another chamber study, coagulation was found to be relevant for ultrafine particles at high number concentrations (above 10^4 cm^{-3}) and turbophoresis played a major role for micron particles (Hussein et al., 2009a,b). Alipchenkov et al. (2009) have also modelled coagulation and deposition and validated it using experimental data for two impeller speeds for micron particles. However, we will focus on submicron particle dynamics under both still and stirred conditions.

To the best of our knowledge, no previous theoretical and experimental study has examined the variation of particle size distribution with time for rough surfaces or a combination of smooth and rough surfaces. In the present study, experiments were done using CsI aerosols in a small scale chamber, which represents a compartment of nuclear containment. Though many radioactive species are released into containment, CsI was selected for aerosol behaviour studies as it poses major threat to the environment. The primary focus was on the evolution of submicron particles with time, considering their harmful effects on human health. A large initial number concentration (~10^5 cm^{-3}) enabled us to study both coagulation and deposition under quiescent and turbulent conditions. Different wall surfaces, viz., plexiglass, concrete and sandpaper were chosen in order to study differences in deposition onto smooth surfaces, rough surfaces, or a combination of both. A generalized model to simulate submicron particle behaviour is proposed that couples the volume conserving semi-implicit coagulation of particles with a deposition model for different surfaces. An analytical solution for dry deposition velocity of submicron particles over different surfaces is proposed, along with an improvement in calculating the velocity boundary layer shift in the existing models for rough surfaces (Lai, 2005; Zhao and Wu, 2006b).

2. Materials and methods

2.1. Experimental setup and measurements

2.1.1. Chamber description

Experiments were conducted in a sealed chamber ($1 \times 1 \times 1.25$ m^3) with smooth plexiglass surface (Fig. 1). The aerosol test chamber was designed with dimensions such that the time required for coagulation of particles in the dry experiments be smaller than their settling time, so that the particles have sufficient time to coagulate as they settle down. The chamber was provided with multiple ports on two walls, ceiling, and floor. An inlet for injecting aerosols and an outlet for sampling aerosols were mounted through the side wall. A fan (diameter 12 in) operating at 900 rpm (revolutions-per-minute) to create turbulent conditions was installed on the ceiling of the chamber. Probes to measure temperature and relative humidity were inserted into the chamber through the ceiling. A vacuum pump for purging the chamber was connected at its base. To conduct experiments on rough surfaces, sandpapers of grade P80 (roughness that might be expected on indoor walls) with average grit size of 200 μm were affixed on all the inner surfaces of the chamber (100% chamber area covered by sandpaper). Further, a reinforced concrete slab (1.2×0.4 m^2) was also fabricated (concrete mix 1:2:4 by volume) and mounted inside the chamber against the wall for experiments with combination of different wall surfaces (~7% chamber area covered by the concrete slab).

2.1.2. Aerosol generation and measurements

In order to conduct the chamber studies, CsI aerosols were generated using an atomizer (TSI Model 3079). A 0.01 M solution of CsI was used for producing wet aerosol particles which were passed through a silica gel denuder to dry the aerosol particles (relative humidity of air in the range of 25–30%). The mode of the particle size produced is between 0.04 μm and 0.06 μm while the geometric standard deviation is between 1.5 and 1.7. In this study, all aerosol particles were assumed to be spherical.

The particle size distributions were measured using a scanning mobility particle sizer (SMPS, TSI model 3936; sample flow rate: 0.3 lpm). Temperature and relative humidity measurements inside the chamber were measured using humidity and temperature transmitter (HMT, Vaisala model 337). Temperature values are recorded in the range of 30ºC–35 °C with the relative humidity vary from 25% to 35%.

2.1.3. Experimental procedure

At the start of each experiment, the chamber was cleaned with a wet cloth and then purged with filtered dry air at a high rate (~35 lpm) using the pump for 2 h to achieve minimal total background concentration (~1000 cm^{-3}). The tubing to the pump was then directly connected to the chamber, thus ventilating the chamber with clean dry air. Aerosol particles were then injected into the chamber for 10 min at a fixed flow rate (4 lpm). The fan was operated at 900 rpm (revolutions per minute) for turbulent condition and was switched off for quiescent conditions.

Each experimental setup was given a tag (listed in Table 1) based on the wall surface and turbulence condition which will be used hereafter to describe a particular condition. For each condition, experiments were conducted at least four times to show that the results were reproducible.

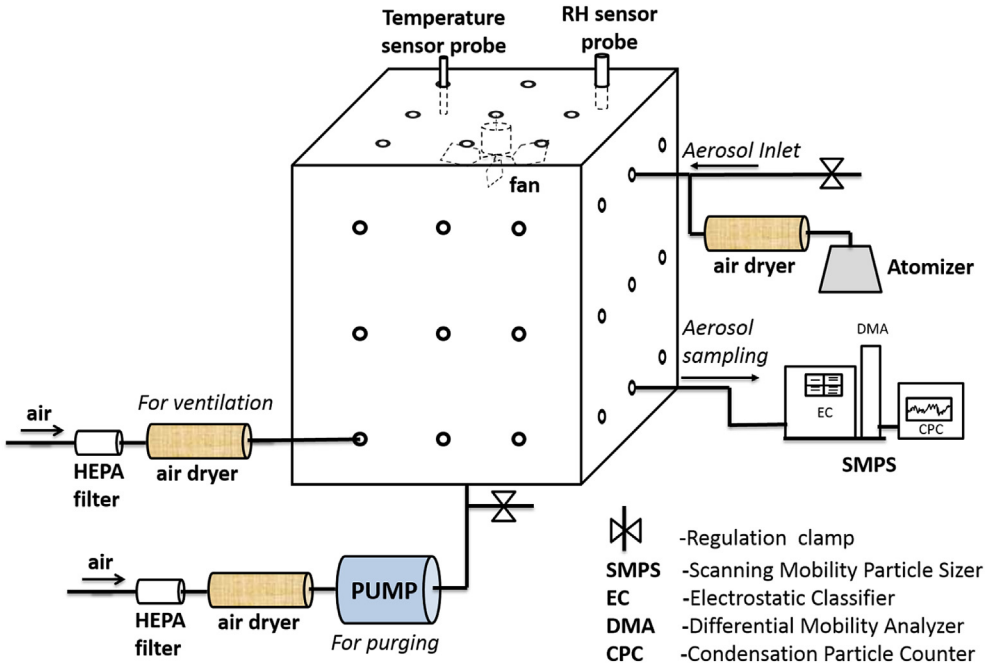

Fig. 1. Schematic of the experimental setup.

Table 1
List of experiment tags under various conditions.

S. No.	Experiment tag	Wall surface	Fan ON/OFF	Roughness (Area covered)
1	PGFOFF	Plexiglass (PG)	OFF	Smooth - 0 μm (100%)
2	PGFON	Plexiglass (PG)	ON	Smooth - 0 μm (100%)
3	SPFOFF	Sandpaper P80 (SP)	OFF	200 μm (100%)
4	SPFON	Sandpaper P80 (SP)	ON	200 μm (100%)
5	CWFOFF	Plexiglass with concrete slab (CW)	OFF	600 μm (~7%)
6	CWFON	Plexiglass with concrete slab (CW)	ON	600 μm (~7%)

2.2. Data analysis and modelling

2.2.1. Modelling coagulation

Coagulation is a significant process for very small particles when the total number concentration is higher than 10^4 cm^{-3} (Hussein et al., 2009a,b). In all our experiments, the initial total number concentration as measured by the SMPS was of the order of 10^5 cm^{-3}, thus making it necessary to model coagulation. The evolution of size distribution of particles as a result of coagulation process is described by the integro-differential equation stated in Eq. (2) (Muller, 1928).

$$\frac{\partial C_{\mathscr{V}}}{\partial t} = \frac{1}{2}\int_0^{\mathscr{V}} \beta_{\mathscr{V}-\overline{\mathscr{V}},\overline{\mathscr{V}}} C_{\mathscr{V}-\overline{\mathscr{V}}} C_{\overline{\mathscr{V}}} d\overline{\mathscr{V}} - C_{\mathscr{V}} \int_0^{\infty} \beta_{\mathscr{V},\overline{\mathscr{V}}} C_{\overline{\mathscr{V}}} C_{\overline{\mathscr{V}}} d\overline{\mathscr{V}} \quad (2)$$

where C is the time dependent number concentration (cm^{-3}) of particles of volume $\mathscr{V}$, $\mathscr{V}-\overline{\mathscr{V}}$ or $\overline{\mathscr{V}}$, and β is the coagulation kernel of two colliding particles. The equation includes both production and depletion of particles of volume $\mathscr{V}$ due to coagulation only.The general formula obtained for volume conserving, semi implicit coagulation of particles of uniform composition is stated in Eq. (3) (Jacobson and Turco, 1994).

$$\mathscr{V}_k C_k^{t+1} = \frac{\mathscr{V}_k C_k^t + \Delta t \sum_{j=1}^{k} \left\{ \sum_{i=1}^{k-1} f_{i,j,k} \beta_{i,j} \mathscr{V}_i C_i^{t+1} C_j^t \right\}}{1 + \Delta t \sum_{j=1}^{N_B} \left(1 - f_{k,j,k}\right) \beta_{k,j} C_j^t} \quad (3)$$

where $\mathscr{V}_k$ is the volume of bin k, C_k^{t+1} is the final number concentration of bin k, C_k^t is the initial number concentration of bin k, Δt is the time step, $\beta_{i,j}$ is the coagulation kernel of colliding particles of bins i and j, $f_{i,j,k}$ is the volume fraction of intermediate particles of volume $\mathscr{V}_i + \mathscr{V}_j$ partitioned to bin k and N_B is the number of bins.

2.2.2. Modelling deposition onto different surfaces

Inside the chamber, the injected aerosols undergo deposition on different surfaces such as ceiling, walls and floor. The deposition velocity is governed by diffusion and gravitational forces. In order to model the deposition velocity, the particle flux through the boundary layer (J), is assumed to be constant through the particle concentration boundary layer and is described below by a modified form of Fick's law (Lai and Nazaroff, 2000).

$$J = \underbrace{-(\varepsilon_p + D)\frac{\partial C}{\partial y}}_{Diffusion} \quad \underbrace{-iv_s C}_{gravitational\ \ settling} \quad (4)$$

where ε_p is the turbulent (eddy) diffusivity of the particle, D is the Brownian diffusivity of the particle, C is the particle concentration

in air, y is the normal distance to the surface, v_s is the settling velocity and i is a constant used to characterize orientation of the surface, $i = 1$ for an upward facing horizontal surface (floor); $i = -1$ for a downward facing horizontal surface (ceiling); $i = 0$ for a vertical surface.

Let C_∞ be the particle concentration outside the concentration boundary layer; the particle deposition velocity (v_d) is defined as follows (Lai and Nazaroff, 2000).

$$v_d = \frac{|J(y=0)|}{C_\infty} \tag{5}$$

For the sake of convenience, particle concentration (C), distance from the surface (y) and deposition velocity (v_d) are normalized by the freestream particle concentration (C_∞), friction velocity (u^*) and fluid kinematic viscosity (ν) as follows in Eqs. (6)–(8).

$$C^+ = \frac{C}{C_\infty} \tag{6}$$

$$y^+ = \frac{yu^*}{\nu} \tag{7}$$

$$v_d^+ = \frac{v_d}{u^*} \tag{8}$$

Using Eqs. (5)–(8) for $i = 0$, Eq. (4) can be written as follows in order to calculate deposition velocity for a wall surface.

$$v_d^+ = \left(\frac{\varepsilon_p + D}{\nu}\right)\frac{\partial C^+}{\partial y^+} \tag{9}$$

Guha (1997) extended his deposition model of smooth surfaces to rough surfaces by assuming that the particles are being captured when they reach the effective roughness height (b).

$$b = k_s - e \tag{10}$$

wherek_s is the roughness height and e is the shift of the velocity boundary layer. Boundary conditions taking the effect of interception on a rough surface have been stated in Eq. (12) (Guha, 1997). Here, $r^+ = (d_p/2)(u^*/\nu)$, where d_p is the particle diameter and

$$b^+ = k^+ - e^+ = b(u^*/\nu) = (k_s - e)(\,u^*/\nu) \tag{11}$$

$$C^+ = \begin{cases} 0 & at\ y^+ = r^+ + b^+ \\ 1 & at\ y^+ = 200 \end{cases} \tag{12}$$

Eq. (9) is re-arranged as follows and its integration across the boundary layer, subject to the boundary conditions stated in Eq. (12) yields the deposition velocity.

$$\frac{1}{v_d^+} = \int_0^1 \frac{dC^+}{v_d^+} = \int_{r^+ + b^+}^{200} \left(\frac{\nu}{\varepsilon_p + D}\right) dy^+ = I \tag{13}$$

Now in order to solve the integration, particle eddy diffusivity is assumed to be equal to the fluid turbulent viscosity (v_t). It has been proved mathematically that $\frac{\varepsilon_p}{v_t} = 1$ for homogeneous isotropic turbulence and for particles with dimensionless relaxation times $\left(\tau_p^+ = \frac{\tau_p u^{*2}}{\nu}\right)$ less than 0.1 (Hinze, 1975). Here τ_p is the particle relaxation time. For our conditions, the dimensionless relaxation times were always found to be less than 0.1($\tau_p^+ \ll 0.1$). The fluid turbulent viscosity is calculated by the correlation stated below (Johansen, 1991).

$$\frac{v_t}{\nu} = \begin{cases} \left(\frac{y^+}{11.15}\right)^3 & y^+ < 3 \\ \left(\frac{y^+}{11.4}\right)^2 - 0.049774 & 3 \le y^+ \le 52.108 \\ 0.4y^+ & y^+ > 52.108 \end{cases} \tag{14}$$

Depending upon the three regimes indicated in Eq. (14), the integral in Eq. (13) was solved analytically for three different cases.

Case I : $r^+ + b^+ < 3$

$$I = \underbrace{\int_{r^+ + b^+}^{3} \frac{dy^+}{\left(\left(\frac{y^+}{11.15}\right)^3 + Sc^{-1}\right)}}_{A} + \underbrace{\int_{3}^{52.108} \frac{dy^+}{\left(\left(\frac{y^+}{11.4}\right)^2 - 0.049774 + Sc^{-1}\right)}}_{B} + \underbrace{\int_{52.108}^{200} \frac{dy^+}{(0.4y^+ + Sc^{-1})}}_{C} \tag{15}$$

where Schmidt number $Sc = \nu D^{-1}$ (16)

The values of the three integrals A, B and C is stated in Eqs. (17)–(23) below.

$$A = 3.71667\ Sc^{2/3}[A_1 - (A_2 + A_3)] \tag{17}$$

$$\text{where } A_1 = \frac{1}{2}\ln\left[\frac{(11.15Sc^{-1/3} + 3)^3}{Sc^{-1} + 0.01947}\right] + \sqrt{3}\tan^{-1}\left[\frac{6 - 11.15Sc^{-1/3}}{11.15\sqrt{3}Sc^{-1/3}}\right] \tag{18}$$

$$A_2 = \frac{1}{2}\ln\left[\frac{(11.15Sc^{-1/3} + (r^+ + b^+))^3}{Sc^{-1} + 7.21398\ \times\ 10^{-4}(r^+ + b^+)^3}\right] \tag{19}$$

$$A_3 = \sqrt{3}\tan^{-1}\left[\frac{2(r^+ + b^+) - 11.15Sc^{-1/3}}{11.15\sqrt{3}Sc^{-1/3}}\right] \tag{20}$$

$$B = \frac{64.98}{B_1}\ln\left|\frac{(52.108 + B_1)(3 - B_1)}{(52.108 - B_1)(3 + B_1)}\right| \tag{21}$$

$$\text{where } B_1 = 11.4\left(0.049774 - Sc^{-1}\right)^{1/2} \tag{22}$$

$$C = 2.5\ln\left|\frac{80 + Sc^{-1}}{20.8432 + Sc^{-1}}\right| \tag{23}$$

Case II : $3 \le r^+ + b^+ \le 52.108$

$$I = \underbrace{\int_{r^+ + b^+}^{52.108} \frac{dy^+}{\left(\left(\frac{y^+}{11.4}\right)^2 - 0.049774 + Sc^{-1}\right)}}_{D} + \underbrace{\int_{52.108}^{200} \frac{dy^+}{(0.4y^+ + Sc^{-1})}}_{C} \tag{24}$$

The value of integral is stated in Eq. (25). The value of C was already stated earlier in Eq. (23).

$$D = \frac{64.98}{B_1} \ln \left| \frac{(52.108 + B_1)((r^+ + b^+) - B_1)}{(52.108 - B_1)((r^+ + b^+) + B_1)} \right| \tag{25}$$

Case III : $r^+ + b^+ > 52.108$

$$I = \int_{r^+ + b^+}^{200} \frac{dy^+}{(0.4y^+ + Sc^{-1})} = 2.5 \ln \left| \frac{80 + Sc^{-1}}{0.4(r^+ + b^+) + Sc^{-1}} \right| \tag{26}$$

Now, the deposition velocity for the wall is obtained as follows.

$$v_{wall} = v_d = \frac{u^*}{I} \tag{27}$$

The velocity for the horizontal surfaces (ceiling and floor) has been calculated in the same way as in Lai and Nazaroff (2000) and is stated in Eqs. (28) and (29). Summary of equations for calculating the dry deposition velocity is shown in Table 5.

$$v_{ceil} = \frac{v_s}{\exp\left(\frac{v_s l}{u^*}\right) - 1} \tag{28}$$

$$v_{floor} = \frac{v_s}{1 - exp\left(-\frac{v_s l}{u^*}\right)} \tag{29}$$

Deposition to all surfaces is assumed to proceed independently and the overall loss rate coefficient (λ_d) is calculated as follows.

$$\lambda_d = \frac{v_{ceil} A_{ceil} + v_{wall} A_{wall} + v_{floor} A_{floor}}{V} \tag{30}$$

The same formula is used for both smooth and rough surfaces. However, in case of smooth surfaces, k^+ is taken to be zero and then the integrals are evaluated (Lai, 2005). In case of combination of smooth and rough surfaces, the velocities are calculated separately and the area of different surfaces are used accordingly. The expression for calculating the overall loss rate coefficient when a rough concrete slab is used inside a smooth plexiglass chamber is stated in Eq. (31). The subscripts *r* and *s* are used for rough and smooth surfaces, respectively. In case of plexiglass with a single concrete slab attached only on one wall surface, $A_{wall,r}$ is ~7% of the total chamber area and accounts for the roughness. In the experiment, concrete surface is not distributed evenly across the chamber but in the model we have included rough surface area for all surfaces of the chamber considered in equation (30) which results in equation (31) below. Now the model considers all the surfaces for any type of rough surface distribution (even or uneven).

$$\lambda_d = \frac{\begin{array}{l} v_{ceil,s} A_{ceil,s} + v_{wall,s} A_{wall,s} + v_{floor,s} A_{floor,s} + \; v_{ceil,r} A_{ceil,r} \\ + v_{wall,r} A_{wall,r} + v_{floor,r} A_{floor,r} \end{array}}{V} \tag{31}$$

2.2.3. An aerosol dynamic model for different surfaces

Eq. (2) includes production and loss terms only due to coagulation. Two more loss terms are added to this equation - due to deposition onto surfaces and ventilation. As we are focusing on submicron particles, turbophoresis is neglected. As the particles are being dried and no phase change is involved, condensation and nucleation are also ignored. All the experiments are conducted at room temperature and the effect of thermophoresis is not considered in the absence of a temperature gradient.

$$\frac{\partial C_{\mathscr{V}}}{\partial t} = \frac{1}{2} \int_0^{\mathscr{V}} \beta_{\mathscr{V}-\mathscr{V},\overline{\mathscr{V}}} C_{\mathscr{V}-\overline{\mathscr{V}}} C_{\overline{\mathscr{V}}} d\overline{\mathscr{V}} - C_{\mathscr{V}} \int_0^{\infty} \beta_{\mathscr{V},\overline{\mathscr{V}}} C_{\overline{\mathscr{V}}} C_{\overline{\mathscr{V}}} d\overline{\mathscr{V}} - (\lambda + \lambda_{d,\mathscr{V}}) C_{\mathscr{V}} \tag{32}$$

Here, $\lambda_{d,\mathscr{V}}$ is the overall deposition rate of particles with volume $\mathscr{V}$ as computed in Eqs. (30) and (31) and λ is the ventilation rate ($\lambda = Q/V$ where Q is the sampling rate of the instruments). They are incorporated in Eq. (3) as follows.

$${}_{\mathscr{V}_k} C_k^{t+1} = \frac{{}_{\mathscr{V}_k} C_k^t + \Delta t \sum_{j=1}^{k} \left\{ \sum_{i=1}^{k-1} f_{i,j,k} \beta_{i,j} {}_{\mathscr{V}_i} C_i^{t+1} C_j^t \right\}}{1 + \Delta t \left(\sum_{j=1}^{N_B} \left(1 - f_{k,j,k}\right) \beta_{k,j} C_j^t + \lambda + \lambda_{d,k} \right)} \tag{33}$$

The particle size distribution obtained from the SMPS, just after ten minutes of aerosol injection will be hereafter referred to as initial or time $t = 0$. The model calculations give the same results independent of the value of time step due to semi-implicit non iterative volume conserving solution. The model simulations require the chamber geometries, friction velocity, mean roughness height of the rough surface and initial particle size distribution inside the chamber as input parameters. The mean surface roughness height of sandpaper was known to be 200 μm and of concrete slab was taken to be 600 μm (S. El Hamdani, 2008).

2.2.4. Revised parameterizations for e^+

Traditional parameterization for $e^+ (= 0.55k^+)$ and the one suggested by Zhao and Wu (2006b), as stated in Eq. (1), over predicted the dry deposition velocity and did not agree with Sippola's experiments. The best curve fitted for Sippola's experimental data was of $e^+ = 0.97k^+$ for Sippola's experiments as opposed to $e^+ = 0.82k^+$ obtained from Eq. (1) for $k^+ = 66.9$ (Zhao and Wu, 2006b). The predictions made with the fitted equation Eq. (1) were however better than those made using the traditional model for these large surface roughness values. It should be noted here that Zhao and Wu have modelled only deposition.

For very small values of k^+, $e^+ \approx 0$ and thus large over predictions in dry deposition velocities were obtained in hydraulically smooth and transition regimes ($k^+ \leq 30$). In these cases, the traditional parameterization simulated better than the parameterization suggested in Eq. (1) which showed almost no shift in the velocity boundary layer. Thus, we decided to check different values of this parameterization and arrive at a new constant value of e^+/k^+ which could help simulate results closer to the experimental data for any value of k^+. Thus, it is decided to check different values of this parameterization to arrive at a new constant value of e^+/k^+ which could simulate results closer to the experimental data for any value of k^+. Since the study shows that the model is sensitive to e^+/k^+ value, multiple iterations of e^+/k^+ ratio for different k^+ was done and calculated the RMSE between experimental and modelled data. Based on the minimum RMSE, the final chosen value for e^+/k^+ is 0.9, which is used for further calculations in

present study and it is also validated for different sets of experimental data shown in Section 3.2. However, this term needs to be recalculated, if the conditions differ from the presently considered work.

3. Results and discussion

3.1. Effect of different wall surfaces

We examined experimentally the effect of different wall surfaces, viz., smooth, rough and a combination of both by plotting time series of normalized number and volume concentrations under turbulent condition (Fig. 3). The initial size distributions and total number concentrations of three experiments (PGFON, CWFON and SPFON) are given below in Fig. 2 and Table 2 respectively.

The initial total number concentrations and the initial size distribution of particle in all our experiments were almost of the same order of ~10^5 cm^{-3} and mode of the distribution at ~0.06 μm as shown in Fig. 2. So the effect of coagulation was similar for all three cases. The detailed model calculation in terms of number concentration was done for above three cases and is described with results in Fig. A1 and Fig. A2 under Appendix C. Normalization was done with respect to the initial number concentration of each experiment to neglect the effect of initial number concentrations. Similarly, the volume concentrations were also normalized with respect to the initial volume concentrations. Turbulent condition was chosen to ensure homogeneous mixing inside the chamber, so that the differences observed in Fig. 3 (a) could be attributed entirely to the differences in deposition velocity for the different surfaces chosen. Assuming no change in particle density, and using the fact that coagulation is volume conserving, we attribute the depletion in volume concentration in Fig. 3 (b) to deposition as well as loss due intake of particles by the instrument.

Fig. 3 clearly shows that the decay in number concentration as well as volume concentration increases with increase in surface roughness of the inner surfaces of the chamber. Comparing experiments PGFON and SPFON, we expect the differences as plexiglass is smoother compared to sandpaper. Owing to the roughness, the thickness of the particle concentration boundary layer is reduced (Zhao and Wu, 2007) and a particle might be stopped at a distance greater than $d_p/2$ from the wall, where d_p is the particle diameter. The shorter stopping distance explains the increase in deposition velocity over a rough surface (Huessin et al., 2012).

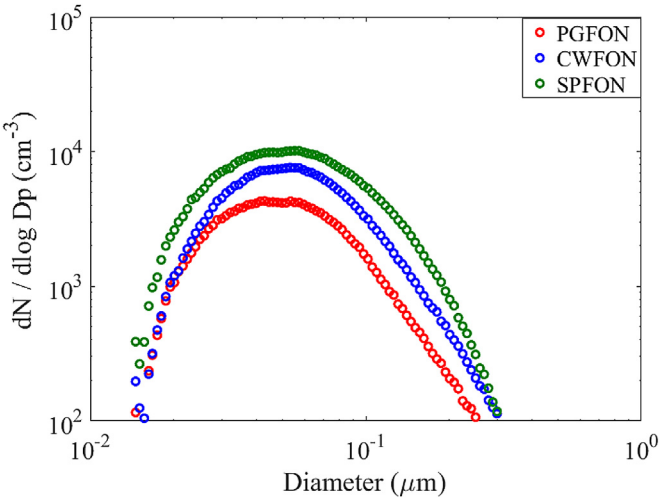

Fig. 2. Initial size distribution of experiments.

Experiments PGFON and CWFON differ in the setup by a concrete slab, which accounts for only ~7% of the inner surface area of the chamber so that significant differences were not expected initially. However, the observed differences are attributed to the large values of surface roughness of the concrete slab, which dominated over the fractional contribution of concrete in the chamber surface area. Comparing experiments CWFON and SPFON, we see that even though the surface roughness of sandpaper is less than that of the concrete slab, the contribution of roughness in terms of area is higher for sandpaper, which shows faster decay in both number as well as volume concentrations.

3.2. Validation of proposed parameterization for e^+

In Fig. 4, the proposed model for calculating deposition velocity is used with different values of e^+/k^+ to compare with the experimental data of Lai and Nazaroff (2005) for four different roughness values of sandpapers (k_s values are 70 μm, 100 μm, 150 μm and 250 μm). For these small values of roughness, it is clearly observed that the proposed value of $e^+/k^+ = 0.9$ performs the best in all four cases. The traditional model ($e^+/k^+ = 0.55$) simulates deposition velocity better than the parameterization suggested by Zhao and Wu (2006b) in Eq. (1). RMSE between the predicted data from the three approaches and the measured data, along with percentage reduction in RMSE after using the proposed approach has been computed and shown in Table 3. Significant reduction in RMSE can be observed when the proposed approach is used compared to the two existing ones.

The depletion in volume concentration is attributed to deposition as well as deposition as well as loss due intake of particles by the instrument as suggested earlier. We plotted the time series of normalized volume concentration of our experimental data (SPFOFF and SPFON) with the simulated data for the above mentioned three parameterizations (Fig. 5). The two different experiments were chosen to represent hydraulically smooth ($k^+ < 3$) and transition regimes ($3 < k^+ < 30$). It is again observed that the proposed approach works better than the previous two approaches and that the traditional parameterization again simulates better than Zhao's parameterization stated in Eq. (1) indicating inefficiency of Zhao's parameterization in case of low roughness values ($k^+ < 30$) in the hydraulically smooth and transition regimes.

Fig. 6 shows that the improved parameterization as suggested by Zhao and Wu (2006b) simulates better than the traditional approach, though both of them do not agree satisfactorily with the measured data for $k^+ = 66.9$. As mentioned earlier, the best agreement was found for $e^+ = 0.97k^+$. In this case also, our proposed parameterization performs better than both the traditional approach and Zhao's approach suggesting that the proposed parameterization predicts the best for different values of k^+. Due to lack of detailed measured data for different roughness values and shift in the velocity boundary layer, Zhao & Wu used the experimental data of Grass (1971) and Wan (1981) in their study and came up with Eq. (1). Due to irregular nature of surface roughness, no universal rule for shift in velocity boundary layer can be derived. However, as discussed in this section, the proposed approach simulates the best results over a wide range of roughness values. Thus, the proposed parameterization is used in the current study to predict the deposition velocity over a rough surface in the aerosol dynamic model.

3.3. Validation of aerosol dynamic model

The aerosol dynamic model proposed in Eq. (32) for submicron

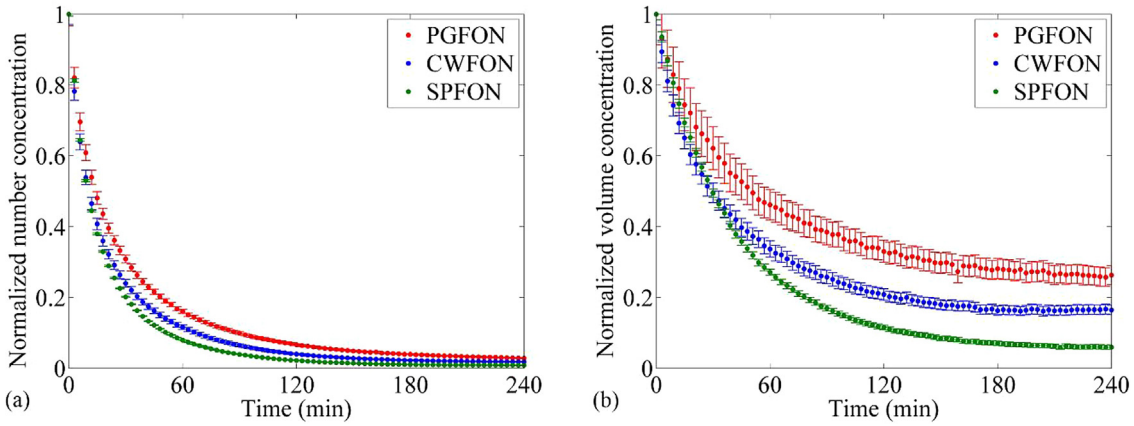

Fig. 3. Time series of normalized number and volume concentration for experiments (plotted at 5% significance level) using different wall surfaces under turbulent condition.

Table 2
Initial total number concentration of experiments.

Experiments	Initial Total Number Concentration
PGFON	1.6112×10^5
CWFON	2.7211×10^5
SPFON	4.135×10^5

particles for smooth, rough, and combination of both surfaces has been validated with the measured data obtained from the experiments done as a part of the current study. Comparison of the model with the measured data for all six conditions (stated in Table 1) is presented in Fig. 6. The effect of turbulence in the experimental data can be clearly seen in all three subplots in Fig. 6. Under turbulent condition (when the fan was switched on), the number concentration has a steeper decay rate compared to quiescent conditions (when the fan was switched off) for all three cases. The differences between quiescent and turbulent conditions for all three wall surfaces are found to be statistically significant with high confidence. These results are expected, as turbulent condition results in a higher value of friction velocity which implies a larger value of inertia, contributing to higher deposition velocity as compared to quiescent conditions (Zhao and Wu, 2007).

The coagulation time scale for polydisperse aerosol with count median diameter (same as geometric mean diameter for lognormal

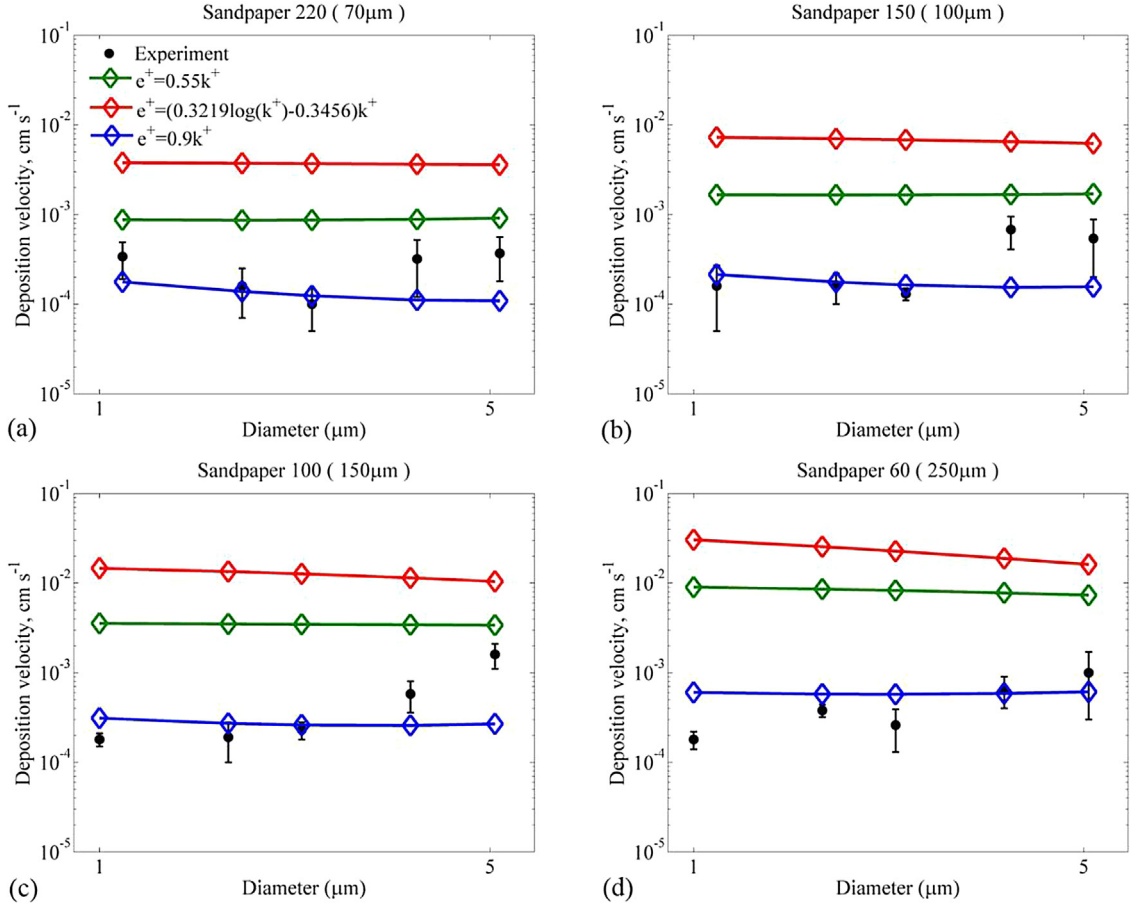

Fig. 4. Comparison of deposition velocities for different values of e^+/k^+ with experimental data of Lai and Nazaroff (2005).

Table 3
RMSE (expressed in 10^{-4} cm s^{-1}) between the model predictions and measured data of Lai and Nazaroff (2005). The values in brackets in last two columns indicate % reduction in RMSE after using our proposed approach.

Sandpaper grade (Roughness value)	Proposed approach ($e^+/k^+ = 0.9$)	Zhao & Wu's approach stated in Eq. (1)	Traditional approach ($e^+/k^+ = 0.55$)
220 (70 μm)	1.67	34.33 (95.1)	6.28 (73.4)
150 (100 μm)	2.93	64.43 (95.4)	13.52 (78.4)
100 (150 μm)	6.17	121.24 (94.9)	29.67 (79.2)
60 (250 μm)	3.07	228.21 (98.7)	77.42 (96.0)

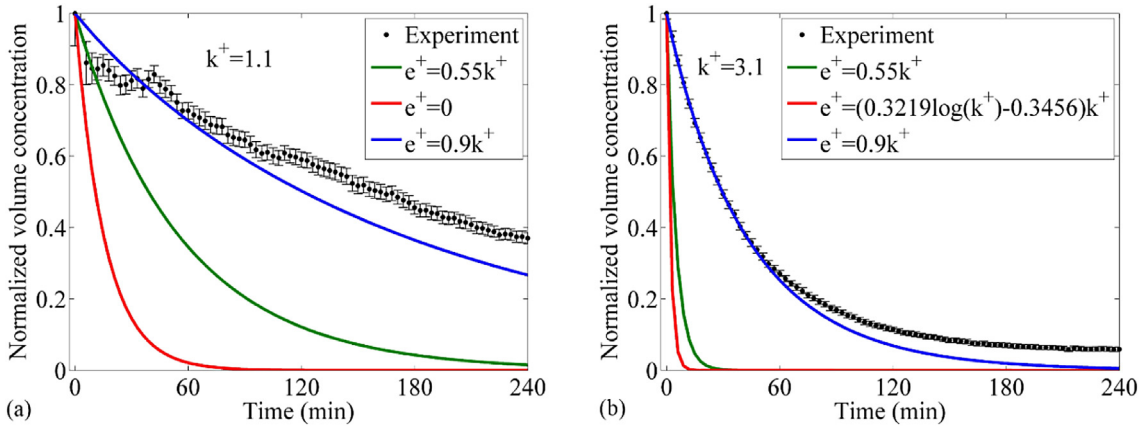

Fig. 5. Comparison of normalized volume concentration for different values of e^+/k^+ with experimental data (a) SPFOFF (b) SPFON.

distribution) 50 nm, geometric standard deviation 1.70 and initial number concentration of the order 10^5 cm^{-3} is calculated to be approximately 30 min. This is observed for quiescent conditions in all three subplots in Fig. 7, which show that coagulation is a dominating process out of deposition and coagulation when the fan is switched off. In both cases, coagulation is the same (The Model results of only coagulation for FAN-OFF and FAN-ON case are shown in Appendix C - Fig. A3) but when the fan is switched off, deposition due to turbulence is not included and deposition is thus less effective. In case of turbulent condition, the number concentration decays faster, and we can see that the number concentration reaches half of its initial value in less than 30 min in all three subplots in Fig. 7. This shows that apart from coagulation, turbulent deposition is also playing a significant role in number concentration decay when the fan is switched on. However, in all these cases, we observe that the number concentration decreases at a very slow pace after two hours. This suggests that out of coagulation and deposition, deposition contributes significantly after two hours as coagulation is less effective due to decrease in total number concentration.

The predictions made by the aerosol dynamic model for all the six conditions agree very well with the measured data. Normalized RMSE is obtained by dividing the RMSE by the range of the measured data and expressed as a percentage, hereafter referred to as NRMSE. NRMSE is calculated for the predicted and measured total number concentrations and varies from 1.17% to 5.36%. Differences between predicted and measured total number concentrations are observed initially for quiescent conditions. These differences are attributed to the inhomogeneous mixing inside the chamber when the fan is not in operation. The model assumes homogeneous mixing and thus simulates the total number concentration really well for turbulent condition. To show that the model is able to capture the aerosol dynamics at different instances, evolution of size distributions for all the six cases is also considered in this study.

Evolution plots for experiments with plexiglass walls are shown in Fig. 8. The mode of the size distribution increases from 57.3 nm to 101.8 nm in 2 h when the fan is switched off and from 42.9 nm to

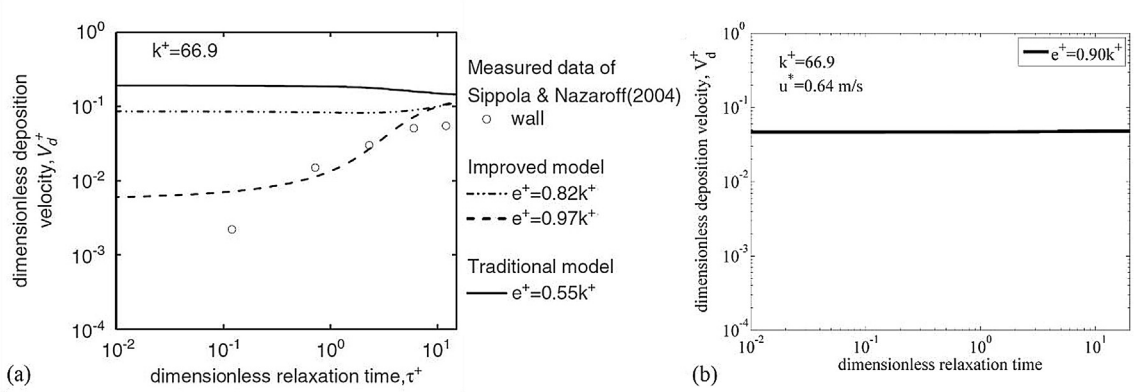

Fig. 6. Comparison of dimensionless deposition velocity of proposed model with measured data and earlier models for large roughness values (a) measured data of Sippola's experiments along with traditional model and Zhao's model (Zhao and Wu, 2006b) (b) proposed model $e^+ = 0.9k^+$.

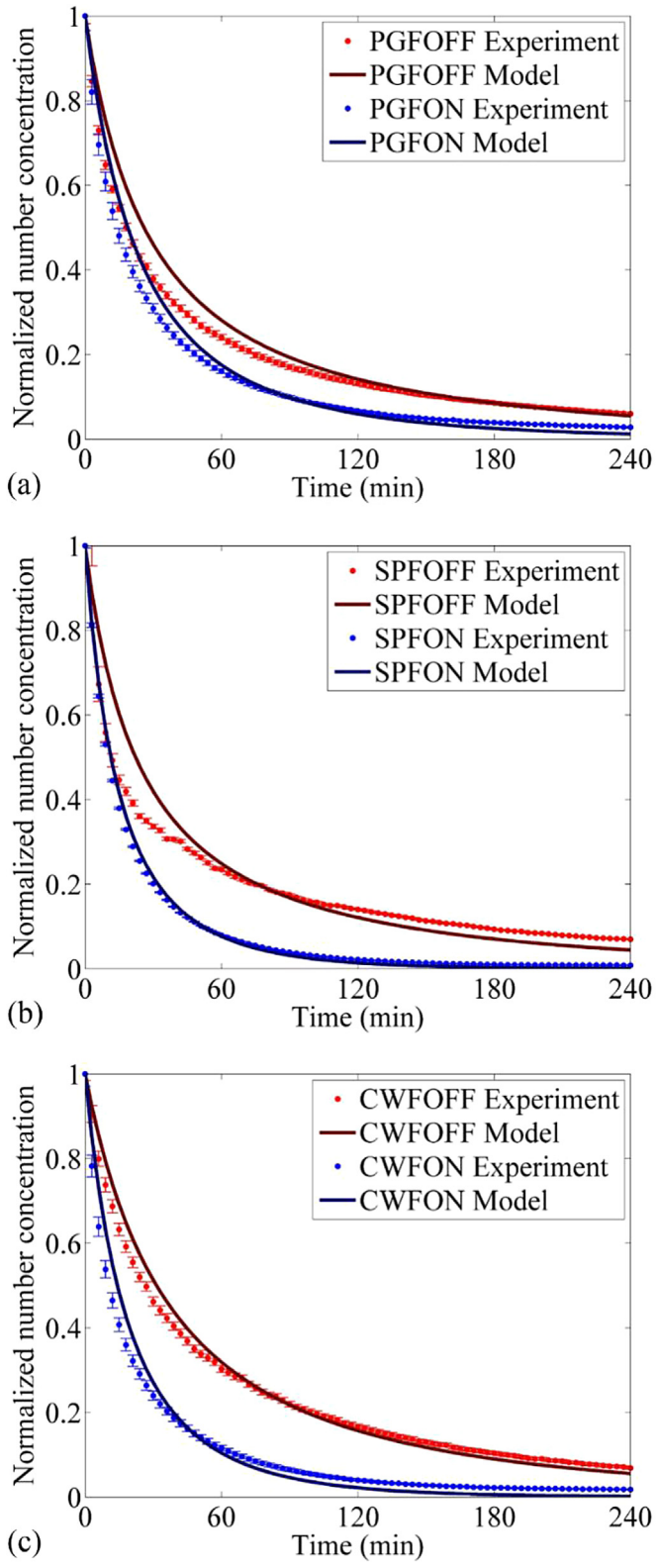

Fig. 7. Comparison of normalized number concentration for both model and experiment (plotted at 5% significance level) under quiescent and turbulent conditions. (a) plexiglass walls, (b) sandpaper (P80) walls, (c) plexiglass with concrete slab.

85.1 nm when the fan is switched on. Here, $Mode_0$ is the mode of the initial size distribution and $Mode_t$ is the mode of the size distribution at time$t$. The ratio of the modes ($Mode_t/Mode_0$) increases with time but the increase is found to be more in case of turbulent condition. This suggests that coagulation is more pronounced when the fan is on. Apart from the shifting of the mode, the peak number concentration decreases faster in experiment PGFON compared to experiment PGFOFF. This is a combined effect of coagulation and turbulent deposition, the latter being dominant. Similar trends are observed in case of sandpaper experiments and those with a concrete slab. To calculate deposition velocity for smooth plexiglass walls, k^+ is taken to be zero. NRMSE between measured and predicted data is as high as 10.49% for quiescent condition and 12.42% for turbulent conditions. The model successfully predicts the head and tail for both the conditions with significant deviations near the mode at 30 min. These differences are attributed to the high deviations in the experimental data. As the chamber is large in size, it takes time to achieve uniformity of number concentration inside the chamber. The model however assumes uniformity of number concentration throughout the chamber at all times and hence we observe differences between modelled and experimental data at 30 min. The differences are observed to reduce with time and the model predicts the same size distribution as measured distribution at 2 h.

Experiments for rough surfaces were done using sandpaper with roughness height$k_s = 200\mu m$. Evolution plots for the same are shown in Fig. 9. NRMSE calculated is as high as 13.61% for both quiescent and turbulent conditions. The model predicts well for turbulent condition and the deviations observed in case of quiescent conditions are attributed to the inhomogeneous mixing in the chamber (see Fig. 10).

Experiments were also done using a concrete slab inside the plexiglass chamber and evolution plots for this combination of smooth and rough surfaces are shown in Fig. 10. NRMSE calculated is as high as 19.00% under turbulent condition and upto 6.87% under quiescent conditions. The model is able to predict the measured size distribution within the error limits (5% significance level) for both cases.

The values of Peak Concentration Reduction Factor (PCRF) has been calculated as the difference of the initial and final concentration of mode of distribution over chosen time interval normalized by the initial number concentration of mode. PCRF for the experimental data are computed for all the six conditions at all four instances and the values are found to be maximum for SPFON (Table 4). Therefore, it is observed that both surface roughness and turbulence increase the dry deposition velocity of particles. We are able to capture both these effects in our proposed model successfully.

4. Summary and conclusions

In this study, experiments were done using CsI aerosols in order to simulate a compartment of Nuclear Reactor Building under accident scenario in a small scale test chamber and evaluate the effect of wall surface and turbulence on aerosol deposition. A generalized model to predict size distribution considering the combined effect of coagulation and deposition is proposed and validated with the measured data. The equations derived to calculate the dry deposition velocity are summarised in Table 4. Following conclusions can be drawn from this study:

(1) Both coagulation and deposition play a significant role for particles in submicron range for high number concentration values (~10^5 cm^{-3}) as is evident from the increase in mode ratio with time and the high peak concentration reduction factors.
(2) Both surface roughness and turbulence increase the deposition velocity, and the maximum effect is observed when

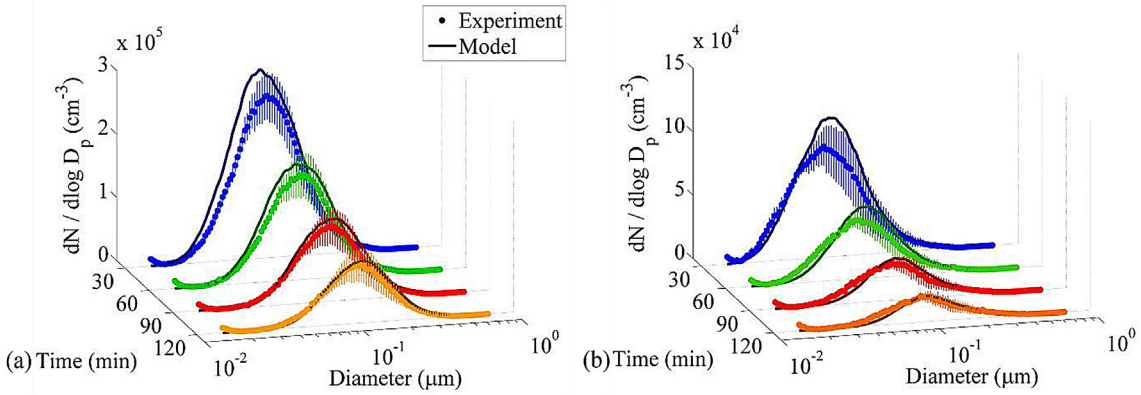

Fig. 8. Comparison of measured (5% significance level) and predicted particle size distribution evolution plots for smooth surfaces under quiescent and turbulent conditions (a) PGFOFF (b) PGFON.

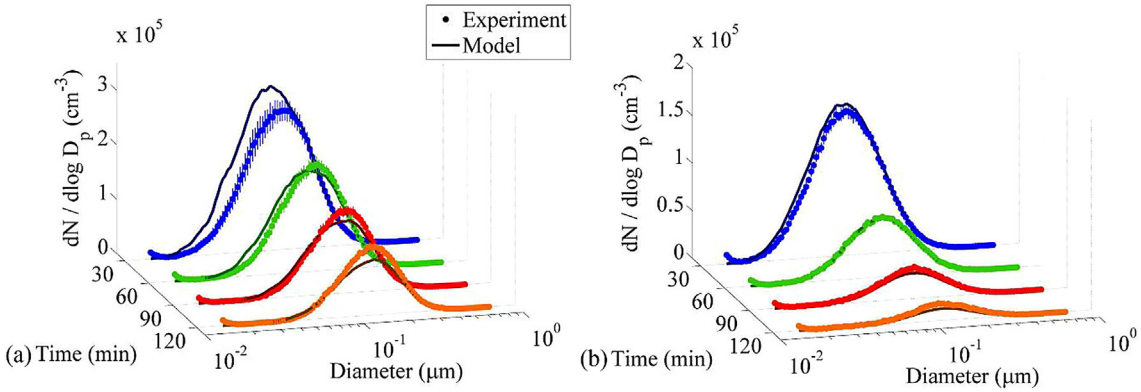

Fig. 9. Comparison of measured (5% significance level) and predicted particle size distribution evolution plots for rough surfaces under quiescent and turbulent conditions (a) SPFOFF (b) SPFON.

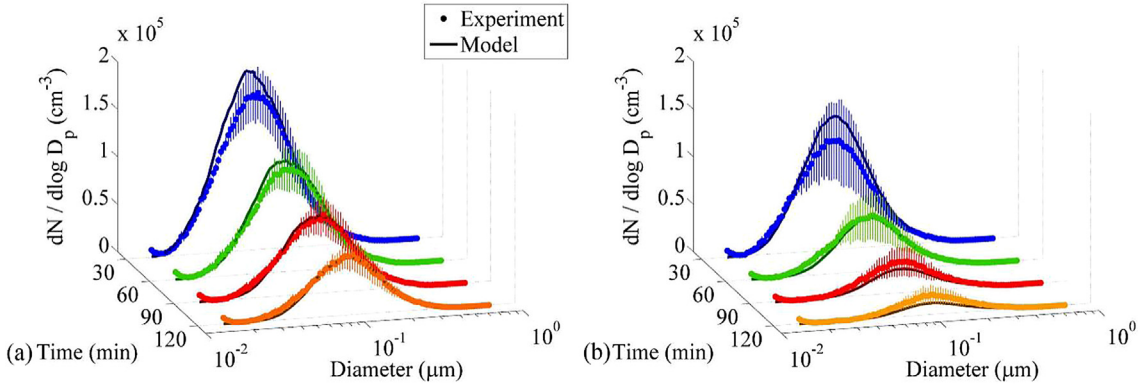

Fig. 10. Comparison of measured (5% significance level) and predicted particle size distribution evolution plots for combination of smooth & rough surfaces under quiescent and turbulent conditions (a) CWFOFF (b) CWFON.

Table 4
PCRF values of experiments at different instances. The value mentioned in subscript denotes *t* minutes. The values are reported in $cm^{-3}\ h^{-1}$.

Experiment	Wall surface	Fan ON/OFF	$PCRF_{30}$	$PCRF_{60}$	$PCRF_{90}$	$PCRF_{120}$
PGFOFF	Plexiglass	OFF	1.381	0.848	0.603	0.468
PGFON	Plexiglass	ON	1.484	0.891	0.632	0.486
SPFOFF	Sandpaper P80	OFF	1.422	0.842	0.605	0.467
SPFON	Sandpaper P80	ON	1.651	0.950	0.655	0.496
CWFOFF	Plexiglass with concrete slab	OFF	1.168	0.755	0.564	0.446
CWFON	Plexiglass with concrete slab	ON	1.585	0.918	0.643	0.490

Table 5
Summary of equations for calculating the dry deposition velocity.

Description	Equation
Deposition velocity, wall	$v_{wall} = \frac{u^*}{I}$
Case I : $r^+ + b^+ < 3$	$I = A + B + C$
	$A = 3.71667\ Sc^{2/3}[A_1 - (A_2 + A_3)]$
	$A_1 = \frac{1}{2}\ln\left[\frac{(11.15Sc^{-1/3}+3)^3}{Sc^{-1}+0.01947}\right] + \sqrt{3}\tan^{-1}\left[\frac{6-11.15Sc^{-1/3}}{11.15\sqrt{3}Sc^{-1/3}}\right]$
	$A_2 = \frac{1}{2}\ln\left[\frac{(11.15Sc^{-1/3}+(r^+ + b^+))^3}{Sc^{-1}+7.21398\times10^{-4}(r^+ + b^+)^3}\right]$
	$A_3 = \sqrt{3}\tan^{-1}\left[\frac{2(r^+ + b^+)-11.15Sc^{-1/3}}{11.15\sqrt{3}Sc^{-1/3}}\right]$
	$B = \frac{64.98}{B_1}\ln\left\lvert\frac{(52.108+B_1)(3-B_1)}{(52.108-B_1)(3+B_1)}\right\rvert$
	$B_1 = 11.4(0.049774 - Sc^{-1})^{1/2}$
	$C = 2.5\ln\left\lvert\frac{80+Sc^{-1}}{20.8432+Sc^{-1}}\right\rvert$
Case II : $3 \le r^+ + b^+ \le 52.108$	$I = C + D$
	$D = \frac{64.98}{B_1}\ln\left\lvert\frac{(52.108+B_1)((r^+ + b^+)-B_1)}{(52.108-B_1)((r^+ + b^+)+B_1)}\right\rvert$
Case III : $r^+ + b^+ > 52.108$	$I = 2.5\ln\left\lvert\frac{80+Sc^{-1}}{0.4(r^+ + b^+)+Sc^{-1}}\right\rvert$
Deposition velocity, ceiling	$v_{ceil} = \frac{v_s}{\exp\left(\frac{v_s I}{u^*}\right)-1}$
Deposition velocity, floor	$v_{floor} = \frac{v_s}{1-\exp\left(-\frac{v_s I}{u^*}\right)}$

$Sc = \nu D^{-1}$, where ν is the kinematic viscosity of air and D is the Brownian diffusivity of particle.
$r^+ = (d_p/2)(u^*/\nu)$, where d_p is the particle diameter and u^* is the friction velocity.
$b^+ = k^+ - e^+$ where k^+ is the dimensionless roughness height and e^+ is the shift in the boundary layer (dimensionless).v_s is the settling velocity.

both the conditions exist together. Peak concentration reduction factor (in 2 h) is found to have the maximum value of 0.496 $cm^{-3}\ h^{-1}$ for SPFON.

(3) The proposed model for predicting aerosol size distribution incorporates an improvement in existing parameterization for estimating shift in velocity boundary layer. This model can be used to calculate dry deposition velocity for smooth, rough surfaces, or combination of both, with the required input parameters being chamber geometry, friction velocity, surface roughness, and initial particle size distribution.
(4) Using the proposed model, the evolution of particle size distribution with time for any kind of surface can also be simulated. This will be helpful to determine number concentrations of a particular size range (at submicron level) at any instance of time.
(5) This study suggests that introducing turbulence has the tendency to reduce the peak aerosol concentration at a faster rate. Besides, coagulation of ultra-fine particles will continue to take place.

According to our knowledge, evolution of submicron particle size distribution due to the combined effect of coagulation and deposition onto rough surfaces has been studied for the first time. The results of this study provide useful insights in minimizing the radioactive fission product release from the containment into the atmosphere.

Acknowledgement

This study is supported by Reactor Safety Division, Bhabha Atomic Research Centre (RSD/RKS/TI/97704/2013-BARC), Trombay, Mumbai. We would like to thank Dr Abhijit Kushari for allowing us to use the photo tachometer. We would also like to thank Deepika, Shamjad and Abhishek for the useful discussions. We also acknowledge Harishankar's assistance at the time of experiments.

Appendix A

The key steps in solving the integration to derive an analytical solution for dry deposition velocity over a rough surface are outlined below,

$$I = \frac{1}{v_d^+} = \int_{r^+ + b^+}^{200} \left(\frac{\nu}{\varepsilon_p + D}\right) dy^+$$

Case I : $r^+ + b^+ < 3$

$$I = \underbrace{\int_{r^+ + b^+}^{3} \frac{dy^+}{\left(\left(\frac{y^+}{11.15}\right)^3 + Sc^{-1}\right)}}_{A} + \underbrace{\int_{3}^{52.108} \frac{dy^+}{\left(\left(\frac{y^+}{11.4}\right)^2 - 0.049774 + Sc^{-1}\right)}}_{B} + \underbrace{\int_{52.108}^{200} \frac{dy^+}{(0.4y^+ + Sc^{-1})}}_{C}$$

$$A = \int_{r^+ + b^+}^{3} \frac{dy^+}{\left(\left(\frac{y^+}{11.15}\right)^3 + Sc^{-1}\right)}$$

$$= \int_{r^+ + b^+}^{3} \frac{(11.15)^3\, dy^+}{\left((y^+)^3 + (11.15Sc^{-1/3})^3\right)}$$

$$\text{Now} \int \frac{dx}{x^3 + a^3} = \frac{1}{3a^2}\left[\frac{1}{2}\ln\frac{(x+a)^3}{x^3+a^3}\right] + \sqrt{3}\tan^{-1}\left(\frac{2x-a}{\sqrt{3}a}\right) + constant$$

where $x = y^+$ and $a = 11.15Sc^{-1/3}$

$$B = \int_{3}^{52.108} \frac{dy^+}{\left(\left(\frac{y^+}{11.4}\right)^2 - 0.049774 + Sc^{-1}\right)}$$

$$= \int_{3}^{52.108} \frac{(11.4)^2\, dy^+}{\left((y^+)^2 - (11.4)^2(0.049774 - Sc^{-1})\right)}$$

Note:

$Sc = \nu/D$ Schmidt number is very small for submicron particles.

For our case $Sc^{-1} \ll 0.049774$, such that $0.049774 - Sc^{-1} > 0$ always.

$$\text{Now} \int \frac{dx}{x^2 - a^2} = \frac{1}{2a}\ln\left|\frac{x+a}{x-a}\right| + constant$$

where $x = y^+$ and $a = 11.4(0.049774 - Sc^{-1})^{1/2}$

$$C = \int_{52.108}^{200} \frac{dy^+}{(0.4y^+ + Sc^{-1})}$$

$$\text{Now} \int \frac{dx}{ax+b} = \frac{1}{a}\ln|ax+b| + constant$$

where $x = y^+$, $a = 0.4$ and $b = Sc^{-1}$

Case II : $3 \le r^+ + b^+ \le 52.108$

$$I = \underbrace{\int_{r^+ + b^+}^{52.108} \frac{dy^+}{\left(\left(\frac{y^+}{11.4}\right)^2 - 0.049774 + Sc^{-1}\right)}}_{\text{D}} + \underbrace{\int_{52.108}^{200} \frac{dy^+}{(0.4y^+ + Sc^{-1})}}_{\text{C}}$$

Integral C has been solved earlier and the integral D is the same as integral B, only the initial and final values are different.

Case III : $r^+ + b^+ > 52.108$

$$I = \int_{r^+ + b^+}^{200} \frac{dy^+}{(0.4y^+ + Sc^{-1})}$$

The above integral is same as integral C with different initial values.

Appendix B

Following is a list of expressions used in the aerosol dynamic model.

Parameter	Equation	
Cunningham slip-flow correction (C_c)	$C_c = 1 + Kn_i[A + Bexp(-CKn_i^{-1})]$ where Knudsen number, $Kn_i = \frac{\lambda_a}{r_i}$	(B1)
	λ_a is the mean free path of an air molecule	
	r_i is radius of particle of size i	
Particle relaxation time (τ_p)	$\tau_p = \frac{C_c \rho_p d_p^2}{18\mu}$ where ρ_p and d_p are particle density and diameter	(B2)
	and μ is molecular dynamic viscosity of air (also η)	
Drag coefficient (C_D)	$C_D = \begin{cases} \frac{24}{Re_p} & Re < 1 \\ \frac{24}{Re_p}(1 + 0.15Re_p^{2/3}) & 1 < Re < 1000 \end{cases}$ where Reynold's number $Re_p = \frac{v_s d_p}{\nu}$	(B3)
	and ν is molecular kinematic viscosity of air	
Settling velocity (v_s)	$v_s = C_c\left(\frac{4}{3}\frac{g d_p}{C_D}\frac{(\rho_p - \rho)}{\rho}\right)^{1/2}$ where ρ is density of air, g is gravitational acceleration	(B4)
Volume fraction ($f_{i,j,k}$), Partitioned into bin k	$f_{i,j,k} = \begin{cases} \left(\frac{\mathscr{V}_{k+1} - \mathscr{V}_{i,j}}{\mathscr{V}_{k+1} - \mathscr{V}_k}\right)\frac{\mathscr{V}_k}{\mathscr{V}_{i,j}} & \le \mathscr{V}_{i,j} < \mathscr{V}_{k+1}; \quad k < N_B \\ 1 - f_{i,j,k-1}\frac{\mathscr{V}_{k-1}}{\mathscr{V}_{i,j}} & < \mathscr{V}_{i,j} < \mathscr{V}_k; \quad k > 1 \\ 1 & \mathscr{V}_{i,j} \ge \mathscr{V}_k; \quad k = N_B \\ 0 & all\ other\ cases \end{cases}$ where $\mathscr{V}_{i,j} = \mathscr{V}_i + \mathscr{V}_j$	(B5)
Particle diffusion coefficient ($D_{p,i}$)	$D_{p,i} = \frac{k_B T}{6\pi r_i \eta} C_c$ where k_B is Boltzmann's constant, T is Kevin temperature	(B6)
Thermal speed of a particle in air ($\bar{v}_{p,i}$)		(B7)

(*continued*)

Parameter	Equation	
	$\overline{v}_{p,i} = \left(\frac{8k_BT}{\pi m_{p,i}}\right)^{1/2}$ where $m_{p,i}$is the mass(g) of one particle of size i	
Mean free path (λ_{pi})	$\lambda_{pi} = \frac{8D_{p,i}}{\pi\overline{v}_{p,i}}$	(B8)
Brownian coagulation kernel ($\beta^B_{i,j}$)	$\beta^B_{i,j} = \frac{4\pi(r_i+r_j)(D_{p,i}+D_{p,j})}{\frac{r_i+r_j}{r_i+r_j+(\delta_i^2+\delta_j^2)^{1/2}} + \frac{4(D_{p,i}+D_{p,j})}{(\overline{v}_{p,i}^2+\overline{v}_{p,j}^2)^{1/2}(r_i+r_j)}}$where $\delta_i = \frac{\{(2r_i+\lambda_{pi})^3-(4r_i^2+\lambda_{pi}^2)^{3/2}\}}{6r_i\lambda_{pi}} - 2r_i$	(B9)
Coagulation kernel due to convective Brownian diffusion enhancement ($\beta^{DE}_{i,j}$)	$\beta^{DE}_{i,j} = \begin{cases} \beta^B_{i,j}0.45Re_j^{1/3}Sc_{p,i}^{1/3}Re_j \le 1, & r_j \ge r_i \\ \beta^B_{i,j}0.45Re_j^{1/2}Sc_{p,i}^{1/3}Re_j > 1, & r_j \ge r \end{cases}$ where Schmidt number $Sc_{p,i} = \frac{\nu_a}{D_{p,i}}$	(B10)
Coagulation kernel due to gravitational collection ($\beta^{GC}_{i,j}$)	$\beta^{GC}_{i,j} = E_{coll,i,j}\pi(r_i+r_j)^2\left\|V_{f,i}-V_{f,j}\right\|$where $V_{f,i}$ is the terminal fall speed(v_s)Collision efficiency, $E_{coll,i,j} = \frac{60E_{V,i,j}+E_{A,i,j}Re_j}{60+Re_j} r_j \ge r_i$	(B11)
	where $E_{V,i,j} = \begin{cases} \left[1+\frac{0.75\ln(2St_{i,j})}{St_{i,j}-1.214}\right]^{-2} & St_{i,j} > 1.214 \\ 0 & St_{i,j} \le 1.214 \end{cases}$ $E_{A,i,j} = \frac{St_{i,j}^2}{(St_{i,j}+0.5)^2}$and $St_{i,j} = \frac{V_{f,i}\left\|V_{f,i}-V_{f,i}\right\|}{r_jg} r_j \ge r_i$	
Coagulation kernel due to turbulent inertial motion ($\beta^{TI}_{i,j}$)	$\beta^{TI}_{i,j} = \frac{\pi\epsilon_d^{3/4}}{g\nu_a^{1/4}}(r_i+r_j)^2\left\|V_{f,i}-V_{f,j}\right\|$	(B12)
Coagulation kernel due to turbulent shear ($\beta^{TS}_{i,j}$)	$\beta^{TS}_{i,j} = \left(\frac{8\pi\epsilon_d}{15\nu_a}\right)^{1/2}(r_i+r_j)^3$	(B13)

Appendix C

We calculated and plotted the normalized number concentration with time, as shown in Fig. A1.

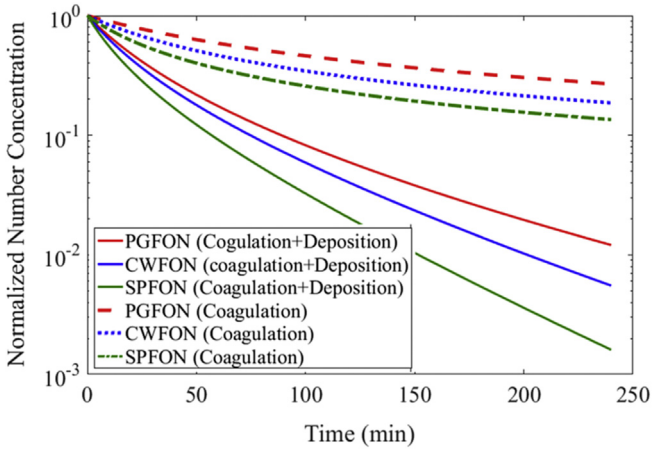

Fig. A1. Comparison between coagulation and coagulation with deposition for the case of a) PGFON, b) CWFON and c) SPFON.

As we expected, the coagulation only results show depletion in number concentration with time, however, after including deposition along with coagulation, rate of depletion becomes much higher for all three cases. The difference in the depletion of number concentration observed in the case of coagulation only is mainly due to the difference in the initial total number concentration of three experiments. However after adding surface dependent deposition the difference between the three cases becomes more due to the effect of different surfaces. So our model results show that coagulation can significantly change the number concentration but with deposition it is heavily increased.

To observed surface dependent deposition clearly in terms of number concentration, we assume same input number concentration for all three cases (PGFON, CWFON, and SPFON). The model results are shown below.

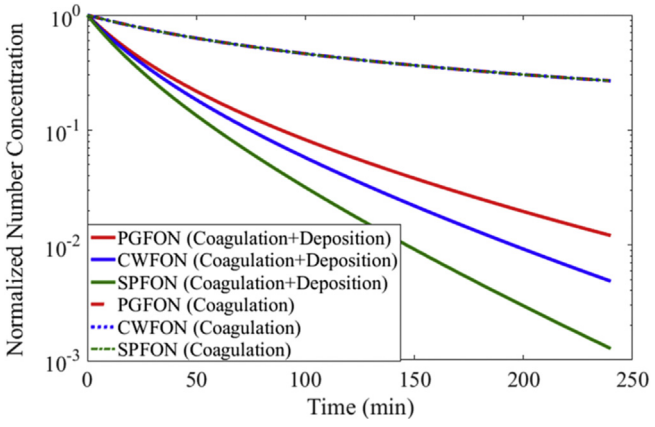

Fig. A2. Comparison between coagulation and coagulation with deposition for the case of a) PGFON, b) CWFON and c) SPFON.

The results show surface dependent deposition plays important role to change the number concentration with time. Fig. A2 above clearly shows that coagulation dependent number concentration depletion is same for all three cases, and significant difference comes from adding deposition on various surfaces. Both Fig. A1 and Fig. A2 above show similar results for the case of surface dependent deposition, so it is indicating that the small difference in the initial number concentration does not contribute much to the final number concentration.

We tested our coagulation model with and without fan for same initial number concentration. The results are shown in Fig. A3.

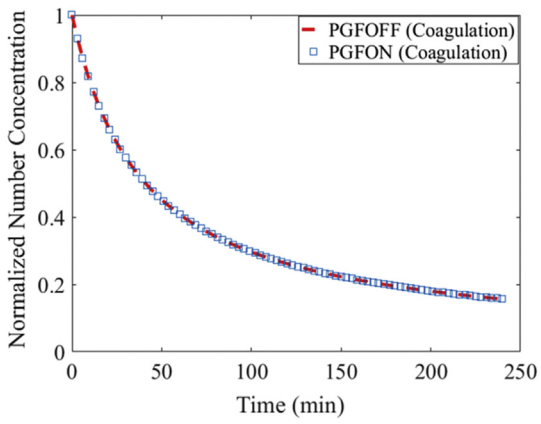

Fig. A3. Coagulation results of PGFOFF and PGFON case.

As we mentioned earlier in the manuscript, results of both cases are same. Major reason is that in our experiments most of particles are less than 1 μm size, at this size range Brownian dependent coagulation is much more higher than all other coagulation (Turbulent shear, Turbulent inertia, Gravitational settling etc.) as mentioned in the "Jacobson, Mark Z. Fundamentals of atmospheric modelling. Cambridge University press, 2005." Also the fan speed is not large enough for creating enough turbulence shear force that can overcome the effect of Brownian coagulation which is present in both cases with and without fan. It only helps in creating a homogenous condition and increases the deposition rate inside the chamber which we have already discussed in detail in the manuscript.

References

Alipchenkov, V.M., et al., 2009. Advancement of Modeling deposition and coagulation of aerosols in a nuclear reactor. Nucl. Eng. Des. 239, 641–647.

Anand, S., et al., 2012. A numerical study of coagulation of nanoparticle aerosols injected continuously into a large, well stirred chamber. J. Aerosol Sci. 52, 18–32.

Brockmann, J.E., Tarbell, W.W., 1984. Aerosol source term in high pressure melt ejection. Nucl. Sci. Eng. 88 (3), 342–356.

Crump, J.G., Seinfeld, J.H., 1981. Turbulent deposition and gravitational sedimentation of an aerosol in a vessel of any shape. J. Aerosol Sci. 12 (5), 405–415.

Fischer, K., Kanzleiter, T., 1999. Experiments and Computational Models for aerosol behaviour in the containment. Nucl. Eng. Des. 191, 53–67.

Grass, A.J., 1971. Structural features of turbulent flow over smooth and rough boundaries. J. Fluid Mech. 50 (2), 233–255.

Guha, A., 1997. A unified Eulerian theory of turbulent deposition to smooth and rough surfaces. J. Aerosol Sci. 28 (8), 1517–1537.

Hinze, J.O., 1975. Turbulence, second ed. McGraw-Hill, New York.

Huessin, T., Smolik, J., Kerminen, V.-M., Kulmala, M., 2012. Modeling dry deposition of aerosol particles onto rough surfaces. Aerosol Sci. Technol. 46 (1), 44–59.

Hussein, T., et al., 2009a. Deposition rates on smooth surfaces and coagulation of aerosol particles inside a test chamber. Atmos. Environ. 43, 905–914.

Hussein, T., et al., 2009b. Deposition of Aerosol particles on Rough surfaces inside a test chamber. Build. Environ. 44, 2056–2063.

Jacobson, M.Z., Turco, R.P., 1994. Modeling coagulation among particles of different composition and size. Atmos. Environ. 28 (7), 1327–1338.

Jacobson, Mark Z., 2005. Fundamentals of Atmospheric Modelling. Cambridge university press.

Johansen, S.T., 1991. The deposition of particle on vertical walls. Int. J. Multiph. Flow. 17 (3), 355–376.

Kim, D.S., Hong, S.B., Kim, Y.J., Lee, K.W., 2006. Deposition and coagulation of polydisperse nanoparticles by Brownian motion and turbulence. J. Aerosol Sci. 37, 1781–1787.

Lai, A.C.K., 2005. Modeling indoor coarse particle deposition onto smooth and rough vertical surfaces. Atmos. Environ. 39, 3823–3830.

Lai, A.C.K., Byrne, M.A., Goddard, A.J.H., 2002. Experimental studies of the effect of rough surfaces and air speed on aerosol deposition in a test chamber. Aerosol Sci. Technol. 36 (10), 973–982.

Lai, A.C.K., Nazaroff, W.W., 2000. Modeling indoor particle deposition from turbulent flow onto smooth surfaces. J. Aerosol Sci. 31 (4), 463–476.

Lai, A.C.K., Nazaroff, W.W., 2005. Supermicron particle deposition from turbulent chamber flow onto smooth and rough vertical surfaces. Atmos. Environ. 39, 4893–4900.

Mayya, Y.S., Sapra, B.K., Khan, A., Sunny, F., 2004. Aerosol removal by unipolar ionization in indoor environments. J. Aerosol Sci. 35, 923–941.

Muller, H., 1928. Kolloïdbeihefte 27, 223.

Piskunov, V.N., 2009. Parameterization of aerosol dry deposition velocities onto smooth and rough surfaces. J. Aerosol Sci. 40, 664–679.

El Hamdani, S., Limam, K., Abadie, M.O., Bendou, A., 2008. Deposition of fine particles on building internal surfaces. Atmos. Environ. 42, 8893–8901.

Sapra, B.K., et al., 2008. Aerosol studies in an Aerosol test facility. Nucl. Technol. 163, 228–244.

Schnell, M., Cheung, C.S., Leung, C.W., 2006. Investigation on the Coagulation and Deposition of Combustion particles in an enclosed chamber with and without stirring. J. Aerosol Sci. 37, 1581–1595.

Shimada, M., Okuyama, K., Kousaka, Y., 1989. Influence of particle inertia on aerosol deposition in a stirred turbulent flow field. J. Aerosol Sci. 20 (4), 419–429.

Shimada, M., Okuyama, K., Kousaka, Y., Seinfeld, J.H., 1988. A model calculation of particle deposition onto a rough wall by Brownian and turbulent diffusion. J. Colloid Interface Sci. 125 (1), 198–211.

Simons, S., Simpson, D.R., 1988. The removal rate for aerosol particles due to the combined effects of diffusion and sedimentation. Ann. Nucl. Energy 15 (3), 161–162.

Sippola, M.R., Nazaroff, W.W., 2004. Experiments measuring particle deposition from fully developed turbulent flow in ventilation ducts. Aerosol Sci. Technol. 38 (9), 914–925.

Slama, M., Shaker, M.O., Aly, R., Sirwah, M., 2014. Applications of aerosol model in the reactor containment. J. Radiat. Res. Appl. Sci. 7, 499–505.

Song, S., et al., 2011. Acute health effects of urban fine and ultrafine particles on children with atopic dermatitis. Environ. Res. 111, 394–399.

Wan, S.G., 1981. Experimental study on turbulence near walls. Chin. Sci. Bull. 26, 1145–1148.

Wood, N., 1981. A simple method for the calculation of turbulent deposition to smooth and rough surfaces. J. Aerosol Sci. 12, 275–290.

Zhao, B., Wu, J., 2006a. Modeling particle deposition from fully developed turbulent flow in ventilation duct. Atmos. Environ. 40, 457–466.

Zhao, B., Wu, J., 2006b. Modeling particle deposition onto rough walls in ventilation duct. Atmos. Environ. 40, 6918–6927.

Zhao, B., Wu, J., 2007. Particle deposition in indoor environments: analysis of influencing factors. J. Hazard. Mater. 147, 439–448.